Published in final edited form as:
Channels (Austin). 2008 ; 2(3): 191–201.

Aromaticity at the water-hydrocarbon core interface of the membrane:

Consequences on the nicotinic acetylcholine receptor

José E. Lizardi-Ortiz[1], **María C. Hyzinski-García**[1], **José L. Fernández-Gerena**[1], **Karen M. Osorio-Martínez**[2], **Eric Velázquez-Rivera**[3], **Félix L. Valle-Avilés**[4], and **José A. Lasalde-Dominicci**[1,*]

[1] College of Natural Sciences; University of Puerto Rico; San Juan, Puerto Rico

[2] Department of Molecular Biology and Genetics; Cornell University; Ithaca, New York USA

[3] Department of Molecular Biology; Genetics and Biochemistry; University of California; Irvine, California USA

[4] School of Medicine; Universidad Central del Caribe; Bayamón, Puerto Rico

Abstract

Almost all lipid-exposed transmembrane domains of integral proteins contain aromatic residues flanking the hydrophobic segment of the domains. These residues generally reside close to the carbonyl region of the membrane, and several structural and functional roles have been associated to these residues. Although the roles and physicochemical reasons for aromatic preference have been extensively studied using model systems, few studies have been done in a native membrane system. To gain insight about the mechanistic implication for this aromatic preference, we selected position αF426 of the muscle-type nicotinic acetylcholine receptor (nAChR). αF426 is a lipid-exposed residue at the extracellular segment of the αM4 transmembrane domain and is highly conserved among different nAChR subunits and species. We used site-directed mutagenesis, α-Bungarotoxin-binding assay, and two-electrodes voltage clamp in *Xenopus laevis* oocytes to characterize mutations at position αF426, which impart different physicochemical properties like volume, polarity, hydrogen bonds, aromaticity and net electrical charge. All mutations except the aromatic residues resulted in a significant reduction of the nAChR cell-surface levels and the macroscopic currents to acetylcholine. These results suggest that position αF426 contributes to structural stability and open-close transitions of the nAChR. Finally, the present study also provides information about how intermolecular interactions at position α426 modulate open-close transitions of the nAChR.

Keywords

nicotinic acetylcholine receptor; lipid-protein interface; water-hydrocarbon core interface; membrane-spanning domain; aromaticity

[*]Correspondence to: José A. Lasalde-Dominicci; Department of Biology; University of Puerto Rico; Río Piedras Campus; P.O. Box 23360; San Juan 00931-3360 Puerto Rico; Tel.: 787.764.0000 exts. 1.2765/4887; Fax: 787.753.3852; joseal@coqui.net/ jlasalde@gmail.com.

Introduction

One feature common to almost all integral membrane proteins is the high occurrence of membrane-exposed aromatic residues (Phe, Trp and Tyr) in regions flanking the hydrophobic segment of transmembrane domains.[1–3] Tryptophan and tyrosine tend to localize at the water-hydrocarbon core interface (WHc interface, also known as polar "head groups") near the carbonyl region of the membrane as has been demonstrated by molecular simulations of integral proteins, high-resolution structural studies of integral proteins, and NMR studies with tryptophan analogs.[4–8] Phenylalanine also tends to be localized at the WHc interface, but can also be accommodated within the hydrocarbon core.[1] Studies on small peptides, tryptophan-analog molecules and simulations studies, suggest that the tendency to be located at the WHc interface arises from a combination of intermolecular interactions and entropic effects associated with the rigid aromatic ring.[4,9–11] It has been proposed that these are mainly van der Waals and cation-π interactions. Dipole interactions and hydrogen bonding contribute to localization but are not essential.

A variety of structural and functional roles have been suggested for the aromatics residues localized at the WHc interface, including membrane anchoring, antiaggregation and cytoprotective antioxidant functions.[12–16] Membrane anchoring is the most studied due to its relation to insertion, orientation and structural and functional stability of transmembrane domains. Studies that have provided insight about this role include (1) electrophysiological and solid-state NMR studies on Gramicidin A showing the importance of four tryptophans for Gramicidin A membrane-insertion stability and Na^+ conductance;[17,18] (2) a simulation study on the KirBac1.1 potassium channel which presents the possible arrangement of aromatic residues in the open and closed states and how these residues contribute to channel stabilization;[19] (3) a kinase-activity assay on the aspartate chemoreceptor which demonstrated the essential role of phenylalanine and tryptophan for structural stability and proper enzymatic function.[20]

However, most previous studies were performed in vitro using membrane or synthetic peptide models, precluding the complexity of the cellular membrane and the diversity of lipid-protein interactions along a native transmembrane domain. Other than a study with small synthetic peptides,[10] there has been no inquiry into physicochemical interactions at this region in a native membrane protein. In the present study, we used the nicotinic acetylcholine receptor (nAChR) as a model membrane protein to examine the consequences of amino acid substitutions at the WHc interface.

nAChR is a member of the Cys-loop superfamily of ligand-gated ion channels and mediates chemical communication at the neuro-muscular junction. nAChR is a heteropentamer composed of four subunits assembled around a fivefold-quasisymmetrical axis (α:β:δ:α:ε). Topologically, each subunit contains an amino-terminal extracellular domain, four α-helix transmembrane domains named M1–M4, a large intracellular loop between M3 and M4, and a short extracellular carboxylic terminal (Fig. 1).[21] The M2 domains of each subunit delimit the ion pore, whereas the M1, M3 and M4 domains flag the outermost limit of the receptor and have the major contact with membrane lipids. nAChR provides an excellent system to study lipid-protein interactions at the WHc interface, because of existing knowledge of channel structure, gating mechanics and the overall spatial orientation of the lipid exposed domains.[21–27]

We introduced a series of amino acid substitutions by site-directed mutagenesis at the position phenylalanine 426 (F426) in the M4 domain of the alpha subunit (Figs. 1 and 2). This position was selected based on the structural model obtained from the *Torpedo marmorata* receptor and labeling studies with hydrophobic and hydrophilic probes.[21,27,28]

The possible role of aromatic residues at this position in the structural or assembly stability of nAChR was examined by means of the α-bungarotoxin (α-BgTx) binding assay, while functionality at the cellular and molecular levels was measured by two-electrode voltage clamp and cell-attached patch clamp, respectively, in *Xenopus laevis* oocytes. Results demonstrated that aromatic residues produced greater stability and functionality for the receptor. The nAChR functionality correlated with the hydrophobicity scale proposed by Wimley and White for the WHc interface.[10] The correlation showed a drastic decrease in receptor functionality on elimination of the aromatic residues and a slow decrease when the residue changed from nonpolar to polar to an amino acid with electrical charge. These results indicate the functional importance of aromaticity in the lipid-protein interactions at the WHc interface, and the possible physiological consequences that a specific mutation at this position could have on nAChR.

Results

Ten point mutations were introduced at the position phenylalanine 426 (F426) of the α subunit, which must be located at the extracellular WHc interface of the M4 transmembrane domain.[21,27,29,30] The mutations were cysteine (F426C), glutamate (F426E), histidine (F426H), lysine (F426K), leucine (F426L), asparagine (F426N), serine (F426S), valine (F426V), tryptophan (F426W) and tyrosine (F426Y). α-BgTx-binding assays, two-electrodes voltage clamp, and single-channel analyses were performed in *X. laevis* oocytes to understand the molecular basis for the conservation of phenylalanine at this position.

Effects of αF426 mutants on cell-surface nAChR levels

Binding assays using [^{125}I] α-BgTx were performed on intact oocytes to determine the cell-surface nAChR level of each mutant and the wild-type. All mutants displayed a decrease in the surface levels in comparison to the wild-type (Table 1). The decrease for each mutant was statistically significant with respect to the wild-type, except for F426S, F426W and F426Y. F426K and F426N binding assays were not significantly different from the nonspecific binding (p values are 0.26 and 0.45, respectively), but both mutants showed similar macroscopic currents (Table 1) that were not observed in noninjected oocytes (data not shown). These data suggested that both mutants produced minimum level of assembled receptors; therefore, they are considered as minimal-assembled receptors. Although the binding for F426E was also not significantly different from the nonspecific binding ($p = 0.07$), its closer value to the rejecting criterion ($p < 0.05$) and its cell-surface level (37% of wild-type) suggested that F426E produced substantial level. Mutant's cell-surface levels decreased in the following order: wild-type > F426S > F426W > F426Y > F426H > F426L > F426V = F426C > F426E > F426K ≈ F426N.

Macroscopic effects of αF426 mutants on receptor activation by acetylcholine

To determine the functionality of the mutant receptors, maximum ACh-induced peak currents (macroscopic mean peak current) were measured by the two-electrode voltage clamp technique. All mutants exhibited a statistically significant change in the mean peak current in comparison to the wild-type (Table 1), with decrease in the peak current ordered as: F426W > wild-type > F426Y > F426V > F426L > F426C > F426S > F426H > F426N ≈ F426E ≈ F426K. These results showed that each of these mutants has the capacity to assemble in functional nAChRs except F426N, F426E and F426K, which have similar macroscopic currents.

To evaluate the responsiveness of the mutant receptors to ACh, the EC_{50} values were determined from concentration-response curves (Fig. 3). The EC_{50} for the wild-type and all mutants are listed in Table 1. All analyzed mutants exhibited a statistically significant

change in the EC_{50} with respect to the wild-type. The F426L showed an increase in EC_{50} (1.2-fold), whereas F426W, F426Y, F426C and F426Y displayed a decrease (1.3, 1.6, 1.6 and 1.9-fold, respectively). The EC_{50} for F426H and F426S were not determined because the mean peak current displayed by these mutants were ≤100 nA (1 of 8 and 3 of 14 oocytes showed currents greater than 100 nA for F426H and F426S, respectively); thus, making difficult to precisely determine this parameter. In addition, when the individual oocytes of each mutant were analyzed, their EC_{50} values were grouped in an ~100 μM range. The Hill slope for all mutants (Table 1) was not significantly different from the wild-type indicating no alteration in the cooperativity of the receptor to ACh.

Effect of the αF426W mutant on the channel opening-closing mechanism

To investigate if the change in macroscopic currents might be explained by an alteration in opening-closing mechanism of the receptor, we performed a single-channel analysis to estimate the kinetic parameters for the wild-type and the F426W mutant using the cell-attach Patch clamp on *X. laevis* oocytes. The αF426W mutant was selected because it had cell-surface level and mean peak current suitable for this kind of analysis. Figure 4 shows single-channel traces, and open-time histograms for wild-type and F426W at 4 μM. The open-time histograms for F426W display a small but statistically significant increase in the mean open time with respect to the wild-type (Table 2). No significant change in channel conductance was observed between the wild-type and F426W (Table 2). Figure 5 shows single-channel traces and open- and close-time histograms for wild-type and F426W at 25 μM and 100 μM, as indicated. Both wild-type and F426W show a displacement to briefer closed times in the closed-time distributions as the concentration of ACh was increased. However, the F426W presented a smaller change in closed-time distribution than the wild-type. The open-time histograms for both wild-type and F426W display a decrease in the mean open time (Table 3) as the ACh concentration increased. Also, F426W presented a small but statistically significant increase in the mean open time at both concentrations of ACh (1.2-fold for 25 μM and 100 μM) with respect to the wild-type.

To identify how the F426W mutant affected the activation process of the channel, microscopic kinetic parameters were determined by fitting simultaneously the following model to the open- and closed-time distributions generated at two ACh concentrations:

$$A+R \underset{k_{-1}}{\overset{k_{+1}}{\rightleftarrows}} A+AR \underset{k_{-2}}{\overset{k_{+2}}{\rightleftarrows}} A_2R \underset{\alpha}{\overset{\beta}{\rightleftarrows}} A_2R^*+B \underset{k_{-b}}{\overset{k_{+b}}{\rightleftarrows}} A_2R^*B$$

In this scheme, A and B are ACh, R is the receptor, AR and A_2R are the monoliganded and biliganded closed states, respectively, A_2R^* is the biliganded open state, and A_2RB^* is the biliganded open state blocked by ACh. $k_{+1}|k_{-1}$ and $k_{+2}|k_{-2}$ are the association|dissociation rate constants for the first and second binding sites, respectively. β is the effective opening rate constant, α is the closing rate constant, and $k_{+b}|k_{-b}$ are the blocking|unblocking rate constants. Table 3 presents the results for the rate constants. F426W mutant slightly altered the opening-closing kinetics of the channel (1.3-fold increase in the effective opening constant and 1.6-fold decrease in the closing constant) with respect to the wild-type. The binding and blocking rate constants displayed minor changes and the open probability value (P_o) for the F426W was slightly increased.

Discussion

Position αF426 is one of the three residues (αD407, αG421 and αF426) that are fully conserved among the residues in αM4 helix of the muscle-type nAChR subunits. Sequence alignment of the M4 domains of different subunits and species (Fig. 2) showed that this

position was highly conserved except for the homomeric subunits (α7–α9), which have a leucine instead of phenylalanine. The high degree of conservation implied that the stability and the proper physiological function of the receptor may be sensitive to physico-chemical properties at this position such as volume, intramolecular or intermolecular interactions, or both. Therefore, the mutants designed for this study were intended to modify these properties.

Based on the most recent nAChR structure and independent labeling studies in M1, M3 and M4 domains, αF426 must reside at the extracellular WHc interface, very close to or within the carbonyl region of the phospholipids (Fig. 1).[21,27,28] According to these studies, the outer lipid-exposed positions that were labeled by the hydrophobic probe 3-trifluoromethyl-3-(*m*-[^{125}I]iodophenyl) diazirine ([^{125}I]-TID) are αL223 (M1 domain), αF284 (M3 domain), and αV425 (M4 domain). On the other hand, the inner lipid-exposed position that was labeled by the hydrophilic probe methanethiosulfonate ethylammonium is αI220 (M1 domain). Furthermore, Unwin's structure (Fig. 1) shows that positions αI220, αF284, αV425 and αF426 display a similar location relative to the membrane bilayer. The heterogeneous labeling pattern by polar and nonpolar probes strongly suggests that these positions must reside at the hydrophilic-hydrophobic interface of the WHc interface. X-ray and neutron diffraction studies of a dioleoylphosphatidylcholine membrane showed that the carbonyl region of the phospholipids displays both hydrophilic and hydrophobic character.[31] This heterogeneous character arises from positional distribution of the phospholipid groups —glycerol backbone, water and the first methylene groups of the acyl chains—along the membrane normal axis. Therefore, we suggest that position αF426 must reside very close to or within the carbonyl region of the membrane, in agreement with the well-established preference of aromatic residues at this position. In addition, Unwin's structure indicates that the lipid-exposed residues αF284 and αF426 are located at the WHc interface, an observation that agrees with the carbonyl-region preference of aromatic residues.

To evaluate the possibility of structural constraint due to change in side-chain volume, the macroscopic parameters—cell-surface nAChR levels and mean peak currents—were analyzed. Previous studies have demonstrated that mutations at the M4 domain did not induce global changes in the ion pore properties—conductance and reversal potential—and agonist binding site kinetics.[22,32–34] On the basis of the ion pore properties, these studies also provided evidence to suggest that mutations did not affect the assembly stoichiometry of the receptors. In addition, a previous study demonstrated that mutations at the agonist binding site did not alter the nAChR affinity for α-BgTx, a results that agrees with a recent structural study on α1 subunit showing that interactions between α-BgTx and alpha subunit is mostly mediated by an N-linked oligosaccharide at position Asn141.[35,36] These results suggest that is very unlikely that mutations at the M4 domain change receptor affinity for α-BgTx and also, provide evidence supporting the use of the α-BgTx-binding assay as a reliable method to measure assembled-nAChR levels of M4-domain mutants in the plasmatic membrane.

Of the ten mutants examined, seven (F426C, F426H, F426L, F426S, F426V, F426W and F426Y) formed functional nAChRs in *X. laevis* oocytes. The tryptophan mutant (largest side chain) had a cell-surface nAChR level similar to the wild-type, and the largest macroscopic current of all mutants. Another study using the *Torpedo californica* nAChR also did not result in drastic changes in cell-surface levels when tryptophan was substituted at lipid-exposed positions within the γM4 domain.[37] A decrease in macroscopic current occurred for all mutants except for F426W. The increase in function and similar surface levels of the tryptophan substitution was not consistent with the view that introducing a bulky amino acid into a position with limited space decreases assembly or activity of the channel.[38] Moreover, the serine substitution produced similar cell-surface levels as the tryptophan substitution;

however, the macroscopic current of the F426S was smaller than F426W. These results indicate that a change in volume at position 426 does not appear to affect nAChR assembly. The present data suggest that other kinds of interactions were responsible for the functional assembly and sensitivity of this position.

Useful information about the nature of the intermolecular interactions can also be obtained from the macroscopic parameters of each mutant. Classifying each side chain by its physicochemical identity and sorting each mutant's cell-surface levels in a descending order, we generated the following list: aromatic (F) > polar (S) > aromatic (W) > aromatic (Y) > polar-charge (H) > nonpolar (L) > nonpolar (V) = polar (C) > charge (E) > charge (K) ≈ polar (N). The ordering of these mutants by the mean peak current was aromatic (W) > aromatic (F) > aromatic (Y) > nonpolar (V) > nonpolar (L) > polar (C) > polar (S) > polar-charge (H). The mutants classified as minimal-assembled or nonfunctional receptors were highly polar (N) or possessed a net electrical charge (E and K). These mutations were not favored because their cell-surface levels (F426N and F426K) and macroscopic currents (F426E, F426K and F426N) were minimal. Correlation of mean peak currents with cell-surface levels of the mutants gave an insight of optimal interactions for proper functioning and stability of the receptor. We hypothesized that aromatic residues were favored followed by nonpolar and then polar residues.

Using WHc interface-localized peptides, Wimley and White created a hydrophobicity scale based on free energy for the whole residues at the WHc interface.[10] They found a residue preference similar to ours (aromatics > nonpolar > polar > charge). Figure 6 presents the correlation between the hydrophobicity scale and the cell-surface nAChR levels (Fig. 6A) and the mean peak currents (Fig. 6B). The values for minimal-assembled and nonfunctional receptors were used in the correlations because their minimal-ACh-induced currents clearly demonstrated that a very small population of these mutants could assemble in functional receptors. The mean peak current fit well with one-phase exponential decay behavior ($R = 0.95$), but the relationship for the cell-surface levels had a low correlation ($R = 0.59$ from linear regression, data not shown); however, tendencies in channel stability and functionality could be identified and predictions could be made.

First, the largest negative free-energies values for aromatic residues agreed with their high cell-surface levels and functionality in comparison with other mutations. Tryptophan had the largest free-energy value of the three residues followed by phenylalanine and then tyrosine. This order was observed for macroscopic current showing high functional sensitivity for aromatic side chains at this position. The decrease in cell-surface levels of tryptophan and tyrosine were not significantly different from the wild-type ($p = 0.169$ and $p = 0.097$, respectively). These results indicate that aromatic residues might have similar cell-surface levels; therefore, the microscopic-kinetic behavior of these mutants could explain their macroscopic behavior.

Second, residues with small free-energy values (positive and negative) induced significant changes in the macroscopic parameters. One-way ANOVA analysis for the macroscopic parameters of the functional nonpolar and polar mutants pointed to similar cell-surface levels ($p = 0.99$), except for serine, and to a slight decrease in the mean peak current ($p < 0.0001$), except for valine. These results suggested that the structures for nonpolar and polar mutant channels are similar and that the physicochemical identity of the residue affected mainly the gating mechanism. The serine mutant had the highest cell-surface level of all mutants. Its very low macroscopic current may have been due to its capacity to make strong hydrogen bonds. Among the nonaromatic mutants, the valine mutant may support a more efficient opening-closing mechanism, as indicated by the increased mean peak current.

Third, residues with large positive free energy values (Asn, Lys and Glu) displayed drastic reductions on the nAChR cell-surface levels (3% and 18% with respect to the wild-type for F426N and F426K, respectively) or mean peak current (F426E, 544-fold decrease from the wild-type). The reduction in nAChR cell-surface levels for the F426N and F426K mutants could arise from impairments in channel assembly, oligomerization or receptor trafficking. Along the same line, F426E, which has similar nAChR cell-surface levels as nonpolar mutants with the largest mean peak currents (F426V, F426L and F426C), displayed the same mean peak current as F426N, implying that this mutation is nonfunctional. On the basis of the macroscopic parameters of these mutants (F426N, F426K and F426E), we suggest that these mutants must induce drastic structural changes in the transmembrane domain affecting the channel stability or receptor gating.

To exclude the possibility that a decrease in macroscopic current was caused by the reduction in the amount of assembled receptor, individual macroscopic currents were normalized by their cell-surface nAChR levels (Fig. 6B; inset). The same macroscopic behavior was observed ($R = 0.98$, one-phase exponential decay) indicating that the decreased current could have been caused by physicochemical properties of the mutants at this position. One such property, hydrophobicity, was evaluated by the mean peak current with the volume of the residue (Fig. 6C), since hydrophobic interactions increase with the size of the nonpolar moiety. Residues with nonpolar side chains and with bulky-carbon-backbone side chains were selected (Leu, Phe, Trp and Val); tyrosine was excluded due to the similarity in volume to phenylalanine. Individual and normalized macroscopic currents for each residue considered (Fig. 6C and inset, respectively) fit well with exponential growth behavior ($R = 0.96$), indicating that the hydrophobic interactions are important for the transition to, or for the stabilization, of the open state. But, based on serine and tyrosine macroscopic parameters, hydrogen bonding may have been involved.

Mutant αF426Y fits the current-hydrophobicity correlation but not the current-volume correlation. Tyrosine and phenylalanine have the same size but tyrosine has an -OH group. The difference in their mean peak currents may be due to the capacity of tyrosine to make hydrogen bonds. At this position, a hydrogen bond with the carbonyl group of the acyl chain could stabilize the helix and the closed conformation, preventing its movement. This explanation could also hold for the serine mutant. The serine and the tyrosine mutants have the same cell-surface level, suggesting that hydrogen bonds stabilize the assembly. The decrease in response of the serine mutant correlated with its greater polarity. The hydrogen bonding ability of some polar residues may override the adverse effect of placing a dipole potential at the WHc interface, as expected from its hydrophobicity index. Although the asparagine mutant had the capacity to make hydrogen bonds, the reduced expression and function must have resulted from its higher dipole moment (3.68 D for Asn versus 1.70 D for Ser).

In addition to the macroscopic parameters–hydrophobicity correlations, the EC_{50} provided further evidence for susceptibility of this position to physicochemical properties of amino acid side chains. The EC_{50} for the functional mutants differed significantly with respect to the wild-type ($p \leq 0.05$). The EC_{50} is an empirical parameter that depends on both the ligand-binding and the opening-closing constants of the nAChR.[39] Previous studies have shown that mutations at the αM4 domain induced minor changes in the binding-kinetic constants; therefore, the observed effects on the EC_{50} are thought to be produced mainly by altering the opening-closing mechanism.[22,34,40]

To gain insight into how the gating process of the channel could be affected by mutations, single-channel analysis was performed on αF426W and wild-type. αF426W was selected because its mean peak current was the closest but significantly different ($p = 0.023$) to the

wild-type. Furthermore, the difference in cell-surface levels between the αF426W mutant and WT was not significant. Therefore, the small difference in the macroscopic current could only be explained in terms of channel gating. As displayed in Tables 2 and 3, the αF426W had a slight increase in the mean open time (τ_o). This increase was due to a decrease in the closing constant (α). This effect, along with the increase in the effective opening constant (β), was reflected in the observed increase of the opening probability (P_o) for αF426W over the wild-type. These results implied that F426W opened faster and efficiently, and that its open state was more stable than that of the wild-type. The blocking and binding constants were slightly affected, consistent with other studies demonstrating that mutations at the αM4 domain do not modify significantly the binding sites or the ion pore.[22,34,40,41] The same effects on the effective opening and closing rate constants produced by αF426W were also observed in another study using choline as the agonist.[25] On the basis of our results and the aforementioned studies, we demonstrated that position αF426 is highly vulnerable to changes in side-chain identity, and that the increase in receptor functionality arises from an optimal channel transition from the closed to the open state; however, allosteric transitions within these domains are also possible and should not be excluded.

A linear free-energy relationship study had proposed that the nAChR gating process occurs as a “conformational wave” model, which propagate from the ligand binding site to the channel gate.[24] This model also proposed that during channel activation the M4 domain moves as a rigid body.[25] On the basis of the typical aromatic preference of the WHc interface, we hypothesized that position αF426 remains at the hydrophilic-hydrophobic interface of the WHc interface all time during the αM4 movement. This idea is based on the following lines of evidence: (1) The membrane-anchoring property of phenylalanine on the transmembrane domain of the M13 major coat protein.[15] (2) Aromatic residues tended to push transmembrane domains toward the interior of the membrane when these residues were situated in the domain away from the hydrocarbon core of the membrane.[42] (3) In KcsA potassium channel, tryptophans located at the WHc interface experienced a slightly change of environment when the hydrophobic length of the membrane was modified.[43] The environment of tryptophans was the same for the conducting and nonconducting states suggesting that aromatics residues remain at a specific membrane location. (4) The effective hydrophobic length of the transmembrane domains was potentially delimited by flanking aromatic residues.[13,14] WHc-interfacial matching of the aromatic residues may have a stronger influence on the location of a transmembrane domain in the membrane than the total hydrophobic matching.

In summary, the structural work on the *T. marmorata* receptor and labeling studies using hydrophilic and hydrophobic probes indicate that the position αF426 is located at the WHc interface. The kind and magnitude of intermolecular interactions of a residue at position αF426 affect several physiological aspects of the channel such as stability, assembling, gating mechanics, and perhaps other aspects not considered in this study (e.g., desensitization). The physicochemical properties of the amino acids residing at this position also correlated with the hydrophobic index proposed by Wimley and White for the WHc interface. Various interactions at this position seem to be responsible for the movement and stabilization of the αM4 domain. Hydrophobic interactions are involved in the transition to or stabilization of the open channel, whereas the hydrogen bonds stabilize the closed conformation. The participation of this position in a variety of interactions is made possible by the dual hydrophobic-hydrophilic nature of the WHc interface. Finally, we hypothesize a role for position α426 in channel gating that needs further studies to verify its certainty and potential importance.

Materials and Methods

Constructs for the muscle-type acetylcholine receptor subunits from mus musculus

cDNA/plasmid encoding the α, β, δ and ε subunits were kindly provided by Dr. A. Auerbach (The State University of New York at Buffalo, NY, USA). The subunit cDNAs were cloned into the EcoRI site of pcDNA3 (Invitrogen, Carlsbad, CA, USA). All subunits are under control of the T7 promoter, except β which is under control of the SP6 promoter.

Generation of mutants at position phenylalanine 426 of the α subunit (αF426)

Site-directed mutagenesis of the αF426 was carried out by codon-mismatch amplification using a QuikChange Site-Directed Mutagenesis kit (Stratagene, La Jolla, CA, USA). The mutagenic primers were designed following the kit's specifications and synthesized by Invitrogen. The mutants were cysteine, glutamate, histidine, lysine, leucine, asparagine, serine, valine, tryptophan and tyrosine. Briefly, amplification reactions were performed in a GeneAmp PCR System 2400 thermal cycler (PerkinElmer, Waltham, MA, USA) for 16 cycles with denaturation for 30 s at 95°C, annealing for 1 min at 55°C, and polymerization for 14 min at 68°C. Forty nanograms of wild-type DNA were used for the PCR reaction. Once completed, the reaction was incubated with 10 units of *Dpn I* at 37°C for 1 h to digest the wild-type vector. The resultant digestion was transformed in TOP10 *Escherichia coli* cell line (Invitrogen). Five colonies were picked randomly, and incubated overnight in Luria Bertani medium with 100 μg/ml of ampicillin (Sigma-Aldrich, St Louis, MO, USA). The plasmids were purified using QIAprep Spin miniprep kit (Qiagen, Valencia, CA, USA). The proper incorporation of the mutants was tested by sequence analysis performed at DBS DNA SEQUENCING FACILITY (University of California, Davis, CA, USA). The DNA sequence was revised using Chromas version 1.45 (http://www.technelysium.com.au).

In vitro RNA transcript synthesis and expression in *Xenopus laevis* oocytes

The cDNA/plasmid for each subunit was linearized by restriction enzyme *EcoRV* for α, δ and ε and *Hind III* for β, and purified by Wizard DNA CleanUp System (Promega, Madison, WI, USA). One microgram of linearized cDNA/plasmid was used as template for in vitro-transcription reaction by mMessenger mMachine kit (Ambion, Austin, TX, USA). Ovarian lobes were obtained from anesthetized female *X. laevis* through a ventral incision about 1 cm in length, and the wounds were closed with two or three stitches of sterile catgut. Follicle cell layers were removed by incubation of the oocytes in Ca^{2+}-free OR2 buffer (82.5 mM NaCl 2.5 mM KCl, 1 mM $MgCl_2$, and 5 mM HEPES, pH 7.6) and 2 mg/ml collagenase for 45 min at room temperature under slow agitation (60 r.p.m.) followed by manual defolliculation. Oocytes of stage V or VI were chosen for injection. A total of 50 ng/oocyte of subunit transcripts at a ratio 2:1:1:1 (α:β:δ:ε) were injected into the cytoplasm of *X. laevis* oocytes. After injection, the oocytes were incubated at 19°C in a medium containing 50% Leibovitz's L-15 media (Invitrogen), 0.4 mg/ml bovine serum albumin (BSA), 0.1 mg/ml Pyruvic Acid and 1X Antibiotic-Antimycotic solution (Sigma-Aldrich). The medium was changed daily.

Total cell-surface nAChR levels

Cell-surface-binding assays using [^{125}I] α-BgTx (PerkinElmer Life Science, Boston, MA, USA) were performed in intact oocytes expressing the αF426 mutants, the wild-type nAChR (48–96 h after injection), and noninjected oocytes (nonspecific-binding control). Each oocyte was incubated in a 50 μl reaction solution containing 20 nM [^{125}I] α-BgTx, 0.5 mg/ml BSA and 1X MOR2 (without EGTA) buffer. The oocytes were incubated for 2 h at room temperature, and then all the oocytes for each mutant were washed with 25 ml of 1X MOR2 (without EGTA) buffer by gravitational filtration. Radioactivity was measured by a γ

counter (Gamma 5500, Beckman, Fullerton, CA, USA). Cell-surface nAChR levels were calculated from a calibration curve that was obtained by counting 0.5–10 μl of a [^{125}I] α-BgTx solution (0.255 fmol/μl).

Voltage clamp recordings and data analysis

Voltage-clamp experiments were performed on oocytes 48–96 h after injection at room temperature using a GeneClamp 500B amplifier (Molecular Devices, Sunnyvale, CA, USA) in the two-electrode voltage clamp configuration. AChR-induced currents were digitally recorded using Clampex 9.0 software (pClamp 9.0, Molecular Devices) on a Pentium IV based computer through a Digidata 1322A interface (Molecular Devices). Microelectrodes were prepared using a PP-830 electrode puller (Narishige, Long Island, NY, USA) with 1.5/0.86 mm (o.d./i.d.) glass capillaries (Sutter Instrument, Novato, CA, USA) and filled with 3 M KCl. Voltage electrode resistance was 2–5 MΩ, and current electrode resistance was lower than the voltage electrode. Voltage clamp recordings were made at a holding potential of −70 mV and filtered at a cut-off frequency of 20 kHz using a Bessel filter. The external buffer was 1X MOR2 (82.5 mM NaCl, 2.5 mM KCl, 1 mM Na_2HPO_4, 5 mM $MgCl_2$, 0.2 mM $CaCl_2$, 0.5 mM EGTA and 5 mM HEPES, pH 7.4). The EGTA was used to chelate the free Ca^{2+} to prevent activation of the Ca^{2+}-activated Cl^- channels. Solutions containing acetylcholine (ACh: 1, 3, 10, 30, 55, 100 and 300 μM) were freshly prepared immediately before each experiment by diluting an 82.55 mM ACh stock solution into MOR2 buffer. Perfusion rates were approximately 30 ml/minute. Concentration-response measurements for wild-type and each mutant were repeated in at least two different batches of oocytes using a minimum of five oocytes. Data points for concentration-response curves were calculated from the peak currents (I) at each concentration using Clampfit 9.0 software (pClamp 9.0). Data points were fitted to the empirical equation: $(I/I_{max}) = (I/I_{max})_{top}/[1 + 10^{HC\ (Log\ EC_{50}\ -\ [ACh])}]$ using GraphPad 4 software (GraphPad Software, San Diego, CA, USA). I_{max} represents the maximum current achieved in each experiment. The Hill coefficient (HC) and the ACh concentration that gave 50% of the maximum normalized response (EC_{50}) were determined from the fitted curve.

Single-channel recording and data analysis

Oocytes expressing the αF426W mutant or the wild-type nAChR (48–96 hours after injection) were transferred to a hypertonic solution composed of 150 mM NaCl, 1 mM KCl, 3% sucrose, and 5 mM HEPES (pH 7.6) for approximately 15 min to induce osmotic shrinkage. The vitelline layer was removed manually, and the oocytes were transferred to the recording chamber containing the bath solution (100 mM KCl, 1 mM $MgCl_2$, 10 mM HEPES, pH 7.2). Patch pipettes were prepared using a P-87 electrode puller (Sutter Instruments) with 1.5/0.86 mm (o.d./i.d.) glass capillaries, and filled with pipette solution (100 mM KCl, 1 mM $MgCl_2$, 10 mM EGTA, 10 mM HEPES, pH 7.2 and 4, 25 or 100 μM of ACh). Single-channel currents were recorded at room temperature using the cell-attached configuration through the Axopatch 200B amplifier (Molecular Device). The signal was filtered at a cut-off frequency of 5 kHz using a Bessel filter, and stored for later analysis on VHS tapes using a VR-10B digital data recorder (Instrutech Corp., Port Washington, NY, USA) and a video recorder. Recorded data were digitized at a sample interval of 20 μs for kinetic and conductance studies using Clampex 10.0 software (pClamp 10.0, Molecular Devices) on a Pentium IV based computer system with a DigiData 1440A digital interface (Molecular Device).

Single-channel conductance and low-concentration mean open times were determined from traces recorded at 4 μM of ACh. The conductance was determined from the slope of the current-voltage graph (I–V graph). To generate the points in the I–V graph three seals for both wild-type or αF426W were recorded at different holding potential (abscissa: 60, 80,

100, 120 and 140 mV). The mean current amplitude (ordinate) was determined from a histogram of the mean amplitude of each event. A trace of approximately 30 s was analyzed for events greater than 1 ms (>200 events) at each holding potential using Clampfit 10.0 (pClamp 10.0). The mean current amplitudes of each seal were averaged, plotted and fitted to a linear equation using GraphPad Prims v.4. The mean open time was determined by selecting open events using the half-amplitude criterion and plotting it in a histogram of the logarithm of open time using Clampfit 10.0. The mean open time was calculated from a logarithmic probability exponential fitting using the variable metric method minimized by the maximum likelihood method.

Single-channel kinetic constants and mean open times were calculated from steady-state recordings at −100 mV using the maximum interval likelihood criterion of the QuB software (www.qub.buffalo.edu). At 25 and 100 μM of Ach, openings corresponding to a single channel cluster as a series of closely spaced events preceded and followed by a closed event greater than a specified duration. This duration was taken as the point of intersection of the predominant duration component and the succeeding component in a closed time histogram. From each patch, clusters containing ten or more openings were selected for analysis. Homogeneity between clusters was analyzed based on the mean open time and open-probability distributions of the clusters.[44] Clusters with mean open times and open probability values within two standard deviations of the mean were selected for further analysis. The resulting open- and closed-duration intervals were analyzed according to a kinetic scheme presented in the results section using the command MIL. Briefly, MIL simultaneously fits recordings obtained at different ACh concentrations, and estimates rate constants in a kinetic scheme using a maximum likelihood method that corrects for missed events.[45] The dead time was set independently for each patch and ranged from 36–42 μs (data not shown). Probability-density functions of open and closed durations were calculated from the fitted rate constants and superimposed on the experimental dwell-time histogram (logarithmic abscissa and a squared root ordinate[46]).

Acknowledgments

This research was supported by in part by grants from the National Institutes of Health RO1GM056371, S06GM008102, SNRP U54NS043011 and UPR Institutional Fund for Research (to José A. Lasalde-Dominicci). We thank the *Decanato de Estudios Graduados e Investigación* of the University of Puerto Rico for financial support offered to José E. Lizardi-Ortiz from 2004 to 2007, and Dr. Sheila Ward for her constructive suggestion in manuscript preparation.

Abbreviations: All amino acids are abbreviated by one or three letters code

WHc interface	water-hydrocarbon core interface
nAChR	nicotinic acetylcholine receptor
cDNA	complementary DNA
ACh	acetylcholine
EC_{50}	concentration at 50 percent of maximum current
τ_o	mean open time
P_o	opening probability
α	closing constant
β	effective opening constant
α-BgTx	α-bungarotoxin

[^{125}I]-TID	3-trifluoromethyl-3-(*m*-[^{125}I]iodophenyl)diazirine
PCR	polymerase chain reaction
BSA	bovine serum albumina

References

1. Landolt-Marticorena C, Williams KA, Deber CM, Reithmeier RA. Non-random distribution of amino acids in the transmembrane segments of human type I single span membrane proteins. J Mol Biol. 1993; 229:602–8. [PubMed: 8433362]
2. von Heijne G. Membrane proteins: from sequence to structure. Annu Rev Biophys Biomol Struct. 1994; 23:167–92. [PubMed: 7919780]
3. Reithmeier RA. Characterization and modeling of membrane proteins using sequence analysis. Curr Opin Struct Biol. 1995; 5:491–500. [PubMed: 8528765]
4. Gaede HC, Yau WM, Gawrisch K. Electrostatic contributions to indole-lipid interactions. J Phys Chem B Condens Matter Mater Surf Interfaces Biophys. 2005; 109:13014–23. [PubMed: 16852615]
5. Deol SS, Bond PJ, Domene C, Sansom MS. Lipid-protein interactions of integral membrane proteins: a comparative simulation study. Biophys J. 2004; 87:3737–49. [PubMed: 15465855]
6. Forrest LR, Tieleman DP, Sansom MS. Defining the transmembrane helix of M2 protein from influenza A by molecular dynamics simulations in a lipid bilayer. Biophys J. 1999; 76:1886–96. [PubMed: 10096886]
7. Tieleman DP, Forrest LR, Sansom MS, Berendsen HJ. Lipid properties and the orientation of aromatic residues in OmpF, influenza M2 and alamethicin systems: molecular dynamics simulations. Biochemistry. 1998; 37:17554–61. [PubMed: 9860871]
8. Lee AG. Lipid-protein interactions in biological membranes: a structural perspective. Biochim Biophys Acta. 2003; 1612:1–40. [PubMed: 12729927]
9. Petersen FN, Jensen MO, Nielsen CH. Interfacial tryptophan residues: a role for the cation-pi effect? Biophys J. 2005; 89:3985–96. [PubMed: 16150973]
10. Wimley WC, White SH. Experimentally determined hydrophobicity scale for proteins at membrane interfaces. Nat Struct Biol. 1996; 3:842–8. [PubMed: 8836100]
11. Yau WM, Wimley WC, Gawrisch K, White SH. The preference of tryptophan for membrane interfaces. Biochemistry. 1998; 37:14713–8. [PubMed: 9778346]
12. Moosmann B, Behl C. Cytoprotective antioxidant function of tyrosine and tryptophan residues in transmembrane proteins. Eur J Biochem. 2000; 267:5687–92. [PubMed: 10971578]
13. de Planque MR, Bonev BB, Demmers JA, Greathouse DV, Koeppe RE 2nd, Separovic F, Watts A, Killian JA. Interfacial anchor properties of tryptophan residues in transmembrane peptides can dominate over hydrophobic matching effects in peptide-lipid interactions. Biochemistry. 2003; 42:5341–8. [PubMed: 12731875]
14. de Planque MR, Kruijtzer JA, Liskamp RM, Marsh D, Greathouse DV, Koeppe RE 2nd, de Kruijff B, Killian JA. Different membrane anchoring positions of tryptophan and lysine in synthetic transmembrane alpha-helical peptides. J Biol Chem. 1999; 274:20839–46. [PubMed: 10409625]
15. Meijer AB, Spruijt RB, Wolfs CJ, Hemminga MA. Membrane-anchoring interactions of M13 major coat protein. Biochemistry. 2001; 40:8815–20. [PubMed: 11467942]
16. Killian JA, Salemink I, de Planque MR, Lindblom G, Koeppe RE 2nd, Greathouse DV. Induction of nonbilayer structures in diacylphosphatidylcholine model membranes by transmembrane alpha-helical peptides: importance of hydrophobic mismatch and proposed role of tryptophans. Biochemistry. 1996; 35:1037–45. [PubMed: 8547239]
17. Becker MD, Greathouse DV, Koeppe RE 2nd, Andersen OS. Amino acid sequence modulation of gramicidin channel function: effects of tryptophan-to-phenylalanine substitutions on the single-channel conductance and duration. Biochemistry. 1991; 30:8830–9. [PubMed: 1716152]

18. Becker MD, Koeppe RE 2nd, Andersen OS. Amino acid substitutions and ion channel function. Model-dependent conclusions. Biophys J. 1992; 62:25–7. [PubMed: 1376168]
19. Domene C, Vemparala S, Klein ML, Venien-Bryan C, Doyle DA. Role of aromatic localization in the gating process of a potassium channel. Biophys J. 2006; 90:01–3.
20. Miller AS, Falke JJ. Side chains at the membrane-water interface modulate the signaling state of a transmembrane receptor. Biochemistry. 2004; 43:1763–70. [PubMed: 14967017]
21. Unwin N. Refined structure of the nicotinic acetylcholine receptor at 4A resolution. J Mol Biol. 2005; 346:967–89. [PubMed: 15701510]
22. Bouzat C, Gumilar F, del Carmen Esandi M, Sine SM. Subunit-selective contribution to channel gating of the M4 domain of the nicotinic receptor. Biophys J. 2002; 82:1920–9. [PubMed: 11916850]
23. Grosman C, Salamone FN, Sine SM, Auerbach A. The extracellular linker of muscle acetylcholine receptor channels is a gating control element. J Gen Physiol. 2000; 116:327–40. [PubMed: 10962011]
24. Grosman C, Zhou M, Auerbach A. Mapping the conformational wave of acetylcholine receptor channel gating. Nature. 2000; 403:773–6. [PubMed: 10693806]
25. Mitra A, Bailey TD, Auerbach AL. Structural dynamics of the M4 transmembrane segment during acetylcholine receptor gating. Structure. 2004; 12:1909–18. [PubMed: 15458639]
26. Shen XM, Deymeer F, Sine SM, Engel AG. Slow-channel mutation in acetylcholine receptor alphaM4 domain and its efficient knockdown. Ann Neurol. 2006; 60:128–36. [PubMed: 16685696]
27. Blanton MP, Cohen JB. Identifying the lipid-protein interface of the Torpedo nicotinic acetylcholine receptor: secondary structure implications. Biochemistry. 1994; 33:2859–72. [PubMed: 8130199]
28. Akabas MH, Karlin A. Identification of acetylcholine receptor channel-lining residues in the M1 segment of the alpha-subunit. Biochemistry. 1995; 34:12496–500. [PubMed: 7547996]
29. Blanton MP, Cohen JB. Mapping the lipid-exposed regions in the *Torpedo californica* nicotinic acetylcholine receptor. Biochemistry. 1992; 31:3738–50. [PubMed: 1567828]
30. Miyazawa A, Fujiyoshi Y, Unwin N. Structure and gating mechanism of the acetylcholine receptor pore. Nature. 2003; 423:949–55. [PubMed: 12827192]
31. Wiener MC, White SH. Structure of a fluid dioleoylphosphatidylcholine bilayer determined by joint refinement of x-ray and neutron diffraction data III. Complete structure Biophys J. 1992; 61:434–47.
32. Lasalde JA, Tamamizu S, Butler DH, Vibat CR, Hung B, McNamee MG. Tryptophan substitutions at the lipid-exposed transmembrane segment M4 of *Torpedo californica* acetylcholine receptor govern channel gating. Biochemistry. 1996; 35:14139–48. [PubMed: 8916899]
33. Ortiz-Miranda SI, Lasalde JA, Pappone PA, McNamee MG. Mutations in the M4 domain of the *Torpedo californica* nicotinic acetylcholine receptor alter channel opening and closing. J Membr Biol. 1997; 158:17–30. [PubMed: 9211718]
34. Bouzat C, Barrantes F, Sine S. Nicotinic receptor fourth transmembrane domain: hydrogen bonding by conserved threonine contributes to channel gating kinetics. J Gen Physiol. 2000; 115:663–72. [PubMed: 10779322]
35. Dellisanti CD, Yao Y, Stroud JC, Wang ZZ, Chen L. Crystal structure of the extracellular domain of nAChR alpha1 bound to alpha-bungarotoxin at 1.94 A resolution. Nat Neurosci. 2007; 10:953–62. [PubMed: 17643119]
36. Tomaselli GF, McLaughlin JT, Jurman ME, Hawrot E, Yellen G. Mutations affecting agonist sensitivity of the nicotinic acetylcholine receptor. Biophys J. 1991; 60:721–7. [PubMed: 1718469]
37. Ortiz-Acevedo A, Melendez M, Asseo AM, Biaggi N, Rojas LV, Lasalde-Dominicci JA. Tryptophan scanning mutagenesis of the gammaM4 transmembrane domain of the acetylcholine receptor from *Torpedo californica*. J Biol Chem. 2004; 279:42250–7. [PubMed: 15247226]
38. Tamamizu S, Guzman GR, Santiago J, Rojas LV, McNamee MG, Lasalde-Dominicci JA. Functional effects of periodic tryptophan substitutions in the alphaM4 transmembrane domain of the *Torpedo californica* nicotinic acetylcholine receptor. Biochemistry. 2000; 39:4666–73. [PubMed: 10769122]

39. Colquhoun D. Binding, gating, affinity and efficacy: the interpretation of structure-activity relationships for agonists and of the effects of mutating receptors. Br J Pharmacol. 1998; 125:924–47. [PubMed: 9846630]
40. Salamone FN, Zhou M, Auerbach A. A re-examination of adult mouse nicotinic acetylcholine receptor channel activation kinetics. J Physiol. 1999; 516:315–30. [PubMed: 10087333]
41. Tamamizu S, Lee Y, Hung B, McNamee MG, Lasalde-Dominicci JA. Alteration in ion channel function of mouse nicotinic acetylcholine receptor by mutations in the M4 transmembrane domain. J Membr Biol. 1999; 170:157–64. [PubMed: 10430659]
42. Braun P, von Heijne G. The aromatic residues Trp and Phe have different effects on the positioning of a transmembrane helix in the microsomal membrane. Biochemistry. 1999; 38:9778–82. [PubMed: 10423258]
43. Williamson IM, Alvis SJ, East JM, Lee AG. Interactions of phospholipids with the potassium channel KcsA. Biophys J. 2002; 83:2026–38. [PubMed: 12324421]
44. Wang HL, Auerbach A, Bren N, Ohno K, Engel AG, Sine SM. Mutation in the M1 domain of the acetylcholine receptor alpha subunit decreases the rate of agonist dissociation. J Gen Physiol. 1997; 109:757–66. [PubMed: 9222901]
45. Qin F, Auerbach A, Sachs F. Estimating single-channel kinetic parameters from idealized patch-clamp data containing missed events. Biophys J. 1996; 70:264–80. [PubMed: 8770203]
46. Sigworth FJ, Sine SM. Data transformations for improved display and fitting of single-channel dwell time histograms. Biophys J. 1987; 52:1047–54. [PubMed: 2447968]
47. Chothia C. Structural invariants in protein folding. Nature. 1975; 254:304–8. [PubMed: 1118010]

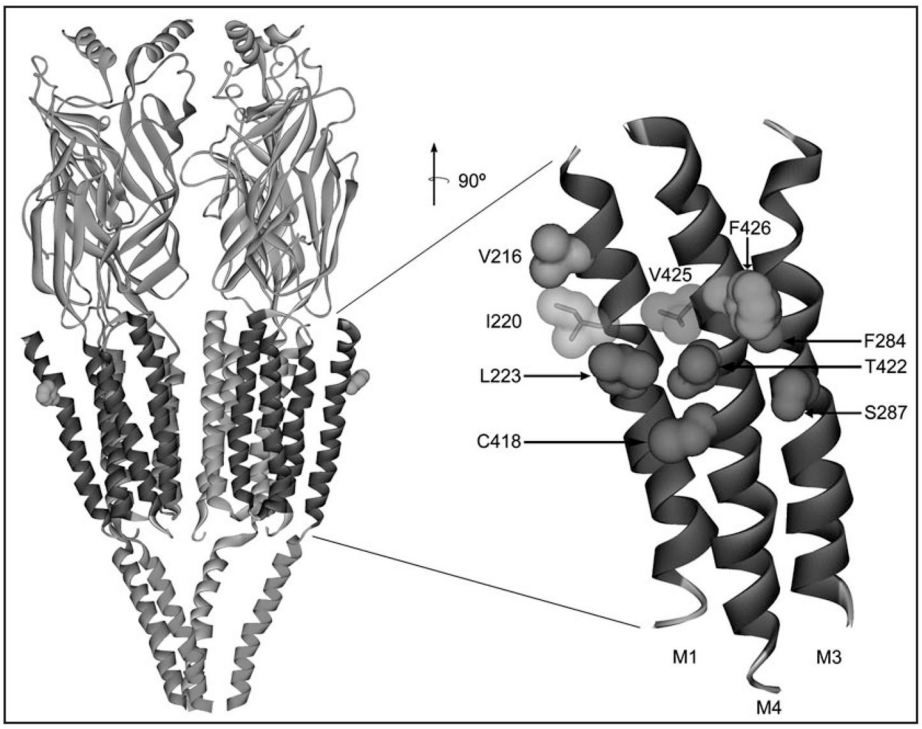

Figure 1.

Molecular model of the muscle-skeletal nicotinic acetylcholine receptor from *M. musculus*. The three-dimensional model was generated with the cryo-electron microscopy data from *T. marmorata* receptor (PDB:2BG9). (Left) The whole receptor viewed from a position parallel to the membrane surface. The α subunits are differentiated by their domains: extracellular domains (light blue), transmembrane domains (red), and the intracellular domain MA (green). The β subunit (purple) and the δ subunit (yellow) are also displayed. The ε subunit located between the two α subunits was omitted for picture clarity. The αF426 position is illustrated as a van der Waals cloud (light green) on each side of the figure. (Right) The lipid-exposed transmembrane domains M1, M3 and M4 after a 90° clockwise rotation through the pore axis to the whole receptor (left). Extracellular-leaflet residues that were labeled by the hydrophobic probe [^{125}I]-TID are displayed in blue, whereas the positions that were labeled by the substituted-cysteine accessibility method (SCAM) are illustrated in gray. The positions I220, F284 and V425 reside in analogous positions on the M1, M3 and M4 domains, respectively. (A color version of this figure is available online.)

				414				418				422				426	
Mouse α	L	G	V	F	M	L	V	C	L	I	G	T	L	A	V	**F**	A
Mouse β	L	W	T	F	I	V	F	T	S	V	G	T	L	V	I	**F**	L
Mouse δ	L	F	V	V	T	P	V	M	V	V	G	T	A	W	I	**F**	L
Mouse ε	F	W	A	A	L	V	L	F	S	V	G	S	T	L	I	**F**	N
Mouse γ	F	L	A	M	L	S	L	F	I	C	G	T	A	G	I	**F**	L
Torpedo α	L	C	V	F	M	L	I	C	I	I	G	T	V	S	V	**F**	A
Human α	L	G	V	F	M	L	V	C	I	I	G	T	L	A	V	**F**	A
Chicken α	L	V	I	F	M	L	V	C	I	I	G	T	L	A	V	**F**	A
Xenopus α	L	A	V	F	M	T	V	C	V	I	G	T	L	A	V	**F**	A
Mouse α4	L	W	M	F	I	I	V	C	L	L	G	T	V	G	L	**F**	L
Mouse α7	L	M	A	F	S	V	F	T	I	I	C	T	I	G	I	**L**	M
Mouse β2	L	W	I	F	V	F	V	C	V	F	G	T	I	G	M	**F**	L

Figure 2.

Sequence alignment of the putative M4 transmembrane domains of the nAChR from different subunits and species. The position αF426 and the corresponding position in other subunits are displayed in bold. This position shows a high degree of conservation between subunits and species, with only the homomeric subtypes (α7–α10) having a different residue (Leu).

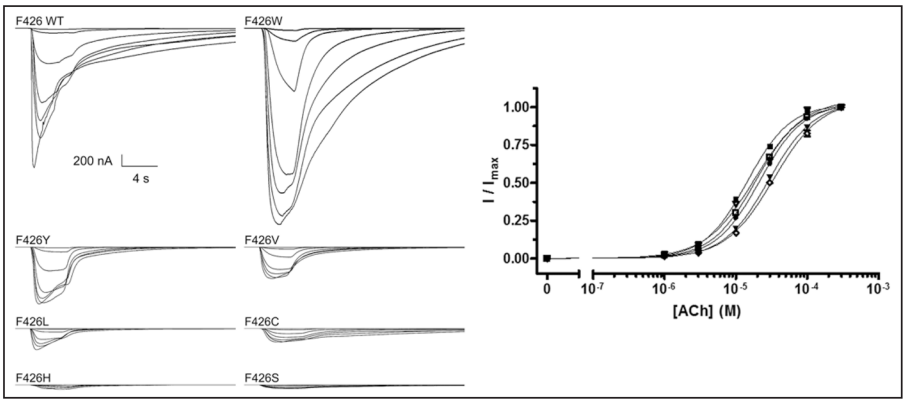

Figure 3.

Representative concentration-response traces (left and middle) and curves (right) for the wild-type (▼), F426C (▽), F426L (◇), F426V (□), F426W (●) and F426Y (■) mutants. Each curve point represents the average peak currents at one particular ACh concentration (seven in total, 1–300 μM) normalized to the maximum peak currents of the corresponding trial. The data representing each mutant were fitted using the Hill equation: $(I/I_{max}) = (I/I_{max})_{top}/[1 + 10^{HC\ (Log\ EC_{50}-\ [ACh])}]$. The abscissa represents ACh concentration (logarithmic scale) and the ordinate represents normalized response. Data points are expressed as mean ± SEM of 8–29 oocytes.

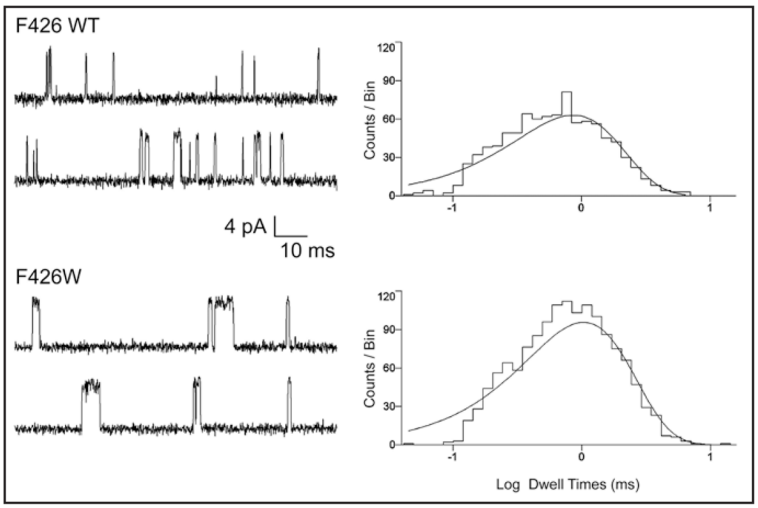

Figure 4.

Single-channel currents (left), and open-time histograms (right) for wild-type and αF426W at low ACh concentration. Continuous-current traces for the corresponding α subunit activated by 4 μM ACh are displayed. Channel openings are presented as upward deflections. All experiments were recorded at a holding potential of −100 mV, sampled at 50 kHz, and filtered at 5 kHz. The Dwell-time histograms were generated using events detected by the half-amplitude criterion. A probability density function was superimposed on to each histogram by means of the variable metric method using maximum likelihood algorithm for minimization. The ordinate represents the events in each bin, and the abscissa is the logarithm (base 10) of the dwell times for the open states.

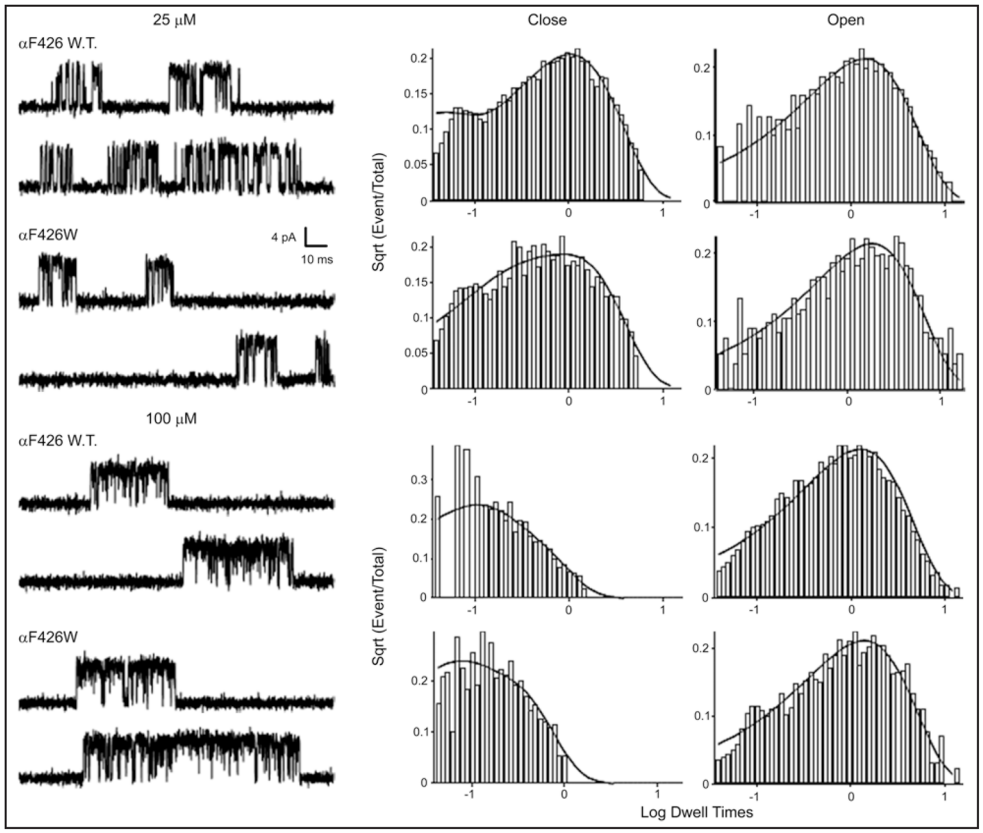

Figure 5.

Single-channel currents (left), closed-time (middle) and open-time (right) histograms for wild-type and αF426W at different ACh concentrations. Continuous-current traces for the corresponding α subunit activated by 25 μM (*top*) and 100 μM (bottom) ACh are displayed. Channel openings are presented as upward deflections. All experiments were recorded at a holding potential of −100 mV, sampled at 50 kHz, and filtered at 5 kHz. The Dwell-time histograms were generated using intraburst times of selected bursts. A probability density function for Scheme was superimposed on to each histogram by means of the maximum interval likelihood algorithm from QuB software (MIL). The ordinate represents the square root of the fraction of total events in each bin, and the abscissa is the logarithm (base 10) of the dwell times for the closed and open states.

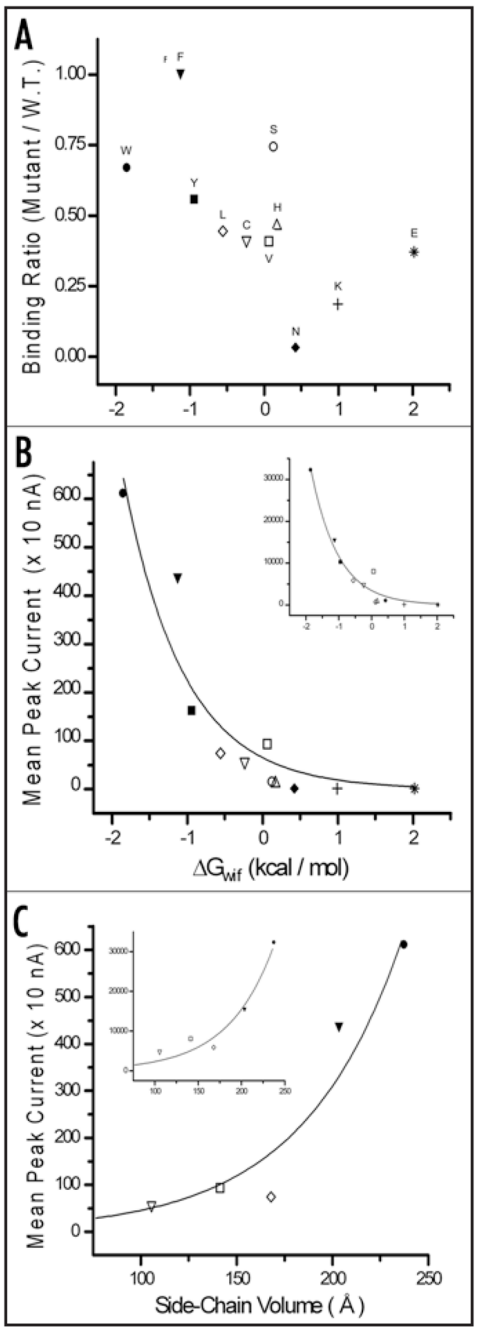

Figure 6.

Correlations of the macroscopic parameters for each mutant with the free energy of amino acid partition (ΔG_{wif}) between water and the water-hydrophobic core interface (top and middle) and with the volume of the side chains (bottom). The mutants are identified as: F426W (●), wild-type (▼), F426Y (■), F426L (◇), F426C (▽), F426V (□), F426S (○), F426H (△), F426N (◆), F426K (+) and F426E (*). (A) Correlation between the expression level and the free energies of partition (ΔG_{wif}) for the mutants. Each point represents the ratio of the mean level for each mutant to the mean level of the wild-type (Table 1). (B) Correlation between the mean peak currents and the free energies of partition (ΔG_{wif}). Each point represents the average of currents at the particular ACh concentration that generated

the maximum peak current. The one-phase exponential decay fit is shown as a solid line. The inset presents the correlation between the mean peak current normalized to mean expression levels and free energies of partition (ΔG_{wif}). (C) Correlation between mean peak currents and side chain volume for the nonpolar mutants and mutants with a large carbon backbone. The only exception is the Cys mutant. Each point represents the average of currents at the ACh concentration that generated the maximum peak current. The exponential growth fit is shown as a solid line. The inset presents the correlation between the mean peak current normalized to mean expression levels and side chain volume of each mutant. The free energies of partition (ΔG_{wif}) for the mutants were obtained from Wimley,[10] and the side chain volumes were obtained from Chontia.[4]

Table 1

Macroscopic parameters for the αF426 mutations

AChR Mutant	EC_{50}[a] (μM)	Hill coefficient[a]	Mean peak current[a] (nA)	Expression ratio[a,b]
F426 W.T.	28.9 ± 1.0	1.37 ± 0.01	4353 ± 541	1
F426C	18.5 ± 1.0*	1.25 ± 0.04	532 ± 118*	0.406◦
F426E	N.D.	N.D.	8 ± 5*	0.371◦
F426H	N.D.	N.D.	74 ± 28*	0.470◦
F426K	N.D.	N.D.	8 ± 2*	0.187†
F426L	33.8 ± 1.0◦	1.30 ± 0.02	742 ± 117*	0.445◦
F426N	N.D.	N.D.	11 ± 1*	0.032*
F426S	N.D.	N.D.	100 ± 31*	0.742
F426V	18.8 ± 1.0*	1.40 ± 0.01	917 ± 124*	0.406◦
F426W	21.6 ± 1.0*	1.42 ± 0.01	6101 ± 512◦	0.667
F426Y	14.5 ± 1.0*	1.45 ± 0.02	1614 ± 235*	0.555

Values are given as the mean ± SEM. N.D. means not determined.

[a] The confidence level for the analyses was 95%.

[b] The expression ratio was calculated from the mutant/wild-type ratio. All parameters were determined using 4–30 oocytes. p values were calculated using a two-tailed, unpaired t test with Welch's correction.

* $p < 0.0001$,

† $p < 0.001$, and

◦ $p \leq 0.05$.

Table 2

Microscopic Parameters for the αF426 W.T. and αF426W

AChR	[ACh] (μM)	Patch/Events[a]	τ_0 (ms)[b]	γ (pS)
F426 W.T.	4	3/1409	1.29 ± 0.03*	97 ± 1
F426W	4	3/920	1.52 ± 0.04*	100 ± 2

Values for the mean open time (τ_O) and channel conductance (γ) are given as the mean ± SEM.

[a] Number of patches/number of events.

[b] The confidence level for the analyses is 95%. P values were calculated using a two-tailed, unpaired t test with Welch's correction.

* $p < 0.0001$.

Table 3

Kinetic parameters for the αF426 W.T. and αF426W

AChR	[ACh] (μM)	Patch/Events[a]	k_{+2}	k_{-2}	β	α	k_{+b}	k_{-b}	Θ[b]	τ_o (ms)[c]	P_o[c]
F426 W.T.	25	3/19017	2900 ± 470	20600 ± 1900	15200 ± 1200	1159 ± 56	433 ± 10	1043 ± 17	13	1.33 ± 0.02*	0.565 ± 0.005*
	100	3/15582								1.20 ± 0.02*	0.877 ± 0.002*
F426W	25	3/2797	2020 ± 370	18600 ± 1900	20000 ± 3100	739 ± 40	312 ± 15	1238 ± 40	27	1.54 ± 0.03*	0.65 ± 0.01*
	100	3/7954								1.46 ± 0.04*	0.901 ± 0.002*

Values are given as the mean ± S.D. except the mean open time (τ_O) and intrabursts open probability (P_O) which is given as mean ± S.E.M.

[a] Number of patches/number of events. The units for rate constants are $\mu M^{-1}\ s^{-1}$ for association constants and s^{-1} for all other rate constants.

[b] Θ is the opening to closing equilibrium constant (β/α).

[c] The confidence level for the analyses is 95%. p values were calculated using a two-tailed, unpaired t-test with Welch's correction.

* $p < 0.0001$.